

## Mechanical properties, *in vitro* and *in vivo* biocompatibility analysis of pure iron porous implant produced by metal injection molding: A new eco-friendly feedstock from natural rubber (*Hevea brasiliensis*)

Diego Pacheco Wermuth<sup>a,1</sup>, Thaís Casagrande Paim<sup>b,1</sup>, Isadora Bertaco<sup>b</sup>, Carla Zanatelli<sup>b</sup>, Liliana Ivet Sous Naasani<sup>b</sup>, Mônica Slaviero<sup>c</sup>, David Driemeier<sup>c</sup>, André Carvalho Tavares<sup>a</sup>, Vinicius Martins<sup>f</sup>, Camila Ferreira Escobar<sup>e</sup>, Luis Alberto Loureiro dos Santos<sup>d</sup>, Lirio Schaeffer<sup>a,2</sup>, Márcia Rosângela Wink<sup>b,\*,2</sup>

<sup>a</sup> Laboratório de Transformação Mecânica, Universidade Federal do Rio Grande do Sul (UFRGS), Av. Bento Gonçalves 9500, 91501-970 Porto Alegre, RS, Brazil

<sup>b</sup> Laboratório de Biologia Celular, Departamento de Ciências Básicas da Saúde, Universidade Federal de Ciências da Saúde de Porto Alegre (UFCSPA), Rua Sarmento Leite 245, 90050-170 Porto Alegre, RS, Brazil

<sup>c</sup> Setor de Patologia Veterinária, Faculdade de Veterinária (FAVET), Universidade Federal do Rio Grande do Sul, Av. Bento Gonçalves 9090, 91540-000 Porto Alegre, RS, Brazil

<sup>d</sup> Laboratório de Biomateriais & Cerâmicas Avançadas, Universidade Federal do Rio Grande do Sul (UFRGS), Av. Bento Gonçalves 9500, 91501-970 Porto Alegre, RS, Brazil

<sup>e</sup> Centro de Ciência e Tecnologia em Energia e Sustentabilidade, Universidade Federal do Recôncavo da Bahia, Av. Centenário 697, 44.085-132 Feira de Santana, BA, Brazil

<sup>f</sup> Laboratório de Metalurgia do Pó, Instituto Federal Sul-rio-grandense Campus Sapucaia do Sul, Av. Copacabana 100, 93216-120 Sapucaia do Sul, RS, Brazil

### ARTICLE INFO

#### Keywords:

Pure iron  
Metal injection molding (MIM)  
Eco-friendly feedstock  
Biodegradable implants  
Adipose-derived mesenchymal stromal cells (ADSCs)  
*In vivo* model of subcutaneous implant

### ABSTRACT

Metal injection molding (MIM) has become an important manufacturing technology for biodegradable medical devices. As a biodegradable metal, pure iron is a promising biomaterial due to its mechanical properties and biocompatibility. In light of this, we performed the first study that manufactured and evaluated the *in vitro* and *in vivo* biocompatibility of samples of iron porous implants produced by MIM with a new eco-friendly feedstock from natural rubber (*Hevea brasiliensis*), a promisor binder that provides elastic property in the green parts. The iron samples were submitted to tests to determine density, microhardness, hardness, yield strength, and stretching. The biocompatibility of the samples was studied *in vitro* with adipose-derived mesenchymal stromal cells (ADSCs) and erythrocytes, and *in vivo* on a preclinical model with Wistar rats, testing the iron samples after subcutaneous implant. Results showed that the manufactured samples have adequate physical, and mechanical characteristics to biomedical devices and they are cytocompatible with ADSCs, hemocompatible and biocompatible with Wistar rats. Therefore, pure iron produced by MIM can be considered a promising material for biomedical applications.

### 1. Introduction

The study of new degradable biomaterials has been one of the most attractive topics in the materials research field [1]. These materials are expected to safely and gradually degrade in the body after their function is served [2]. Metals comprise an important class of degradable biomaterials, because of their suitable mechanical properties in structural

components. Iron (Fe), Magnesium (Mg), Zinc (Zn), Molybdenum (Mo), and Tungsten (W) have been studied to be used as temporary orthopedic, vascular implants, and electronic systems [3].

Previous studies have shown that pure iron can be an appropriate material for biomedical applications [4–6]. Iron has great radial strength due to its high elastic modulus [7] and it is biocompatible. Studies have shown that pure iron stents produced by laser cutting did

\* Corresponding author at: Universidade Federal de Ciências da Saúde de Porto Alegre–UFCSPA, 245, Sarmento Leite, Porto Alegre, RS CEP 90050-170, Brazil.  
E-mail address: [mwink@ufcspa.edu.br](mailto:mwink@ufcspa.edu.br) (M.R. Wink).

<sup>1</sup> These authors contributed equally to this work

<sup>2</sup> These authors shared senior authorship

<https://doi.org/10.1016/j.msec.2021.112532>

Received 14 April 2021; Received in revised form 15 October 2021; Accepted 1 November 2021

Available online 5 November 2021

0928-4931/© 2021 Elsevier B.V. All rights reserved.

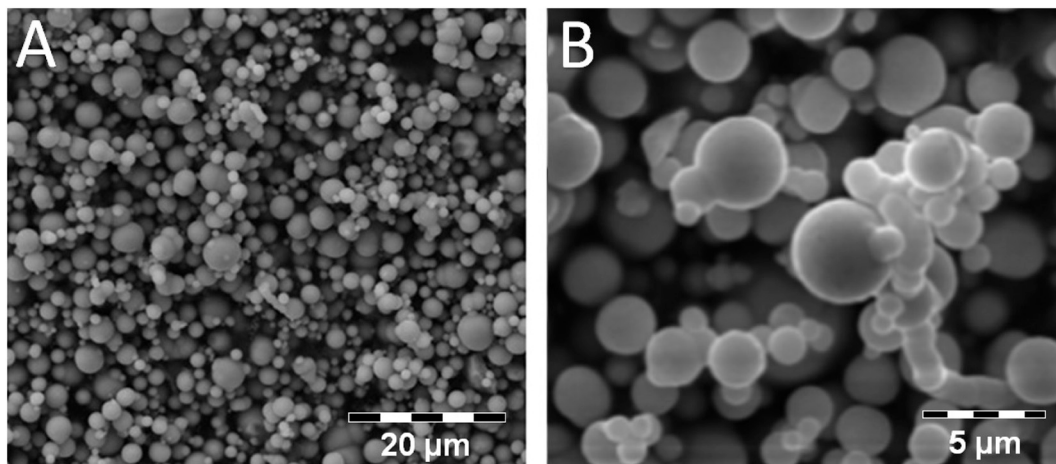


Fig. 1. Iron powder. 99.95% iron powder SEM with a magnification of 3160× (A) and 10,000× (B).

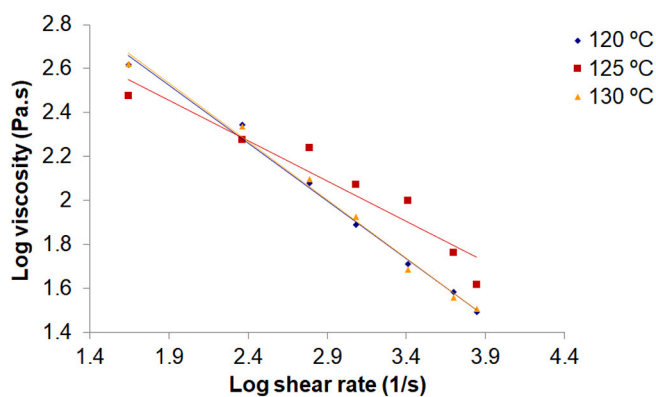


Fig. 2. Rheological evaluation of eco-friendly feedstock. Rheology results at temperatures of 120 °C, 125 °C and 130 °C of feedstock.

Table 1  
Rheological results of the feedstock at 120 °C.

Shear rate (1/s)	Viscosity (Pa.s)	Shear stress (Pa)
44	414.2	24,981
230	221.45	50,933
613	119.44	73,217
1210	77.25	93,475
2560	51.44	131,675
5000	38.37	191,875
7000	31.02	232,675

not cause systemic toxicity, iron overload, and significant inflammatory response in animals [4,5,8].

Iron is a biodegradable metal, whose degradation process involves the oxidation of ferrous ions and their dissolution in body fluids [9,10]. Under physiological conditions, the bioavailability of iron is limited because the soluble ( $Fe^{2+}$ ) (heme) is readily oxidized to ( $Fe^{3+}$ ) (non-heme iron), which is virtually insoluble. The electrons from the anodic reaction are consumed by a corresponding cathodic reaction (1) and the oxygen is reduced and dissolved in water (2). The metals ions ( $Fe^{2+}$ ) react with the hydroxyl ion (OH) and form insoluble hydroxides, which are the most common corrosion products (3–4) [11–13]:

- (1)  $Fe \rightarrow Fe^{2+} + 2e^-$  (anodic reaction)
- (2)  $O_2 + 2H_2O + 4e^- \rightarrow 4OH^-$  (cathodic reaction)
- (3)  $Fe^{2+} + 2OH^- \rightarrow Fe(OH)_2$
- (4)  $4 Fe(OH)_2 + O_2 + 2H_2O \rightarrow 4Fe(OH)_3$  or  $2Fe_2O_3 \cdot 6H_2O$

The ability to donate and accept electrons can lead to significant oxidative damage. The iron overload can produce free radicals and induce damage in different organs such as the pancreas, liver, thyroid, and heart. In the central nervous system, it has been associated with neurodegenerative disorders, such as Parkinson's and Alzheimer's disease [14–16].

An important aspect related to iron is the choice regarding its purity. In a previous study, we compared the mechanical properties and biocompatibility of 99.5% and 99.95% iron samples produced by powder metallurgy. We found that both purity grades have adequate properties to be used in biomedical devices, however, the 99.95% iron had better performance when the biocompatibility was tested *in vitro* [6].

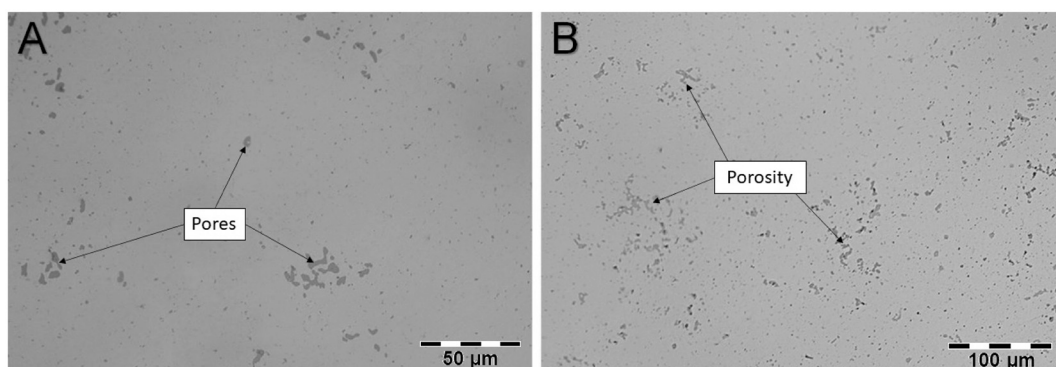


Fig. 3. Porosity. Metallography of sintered pure iron sample with 500× (A) and 200× (B) magnification.

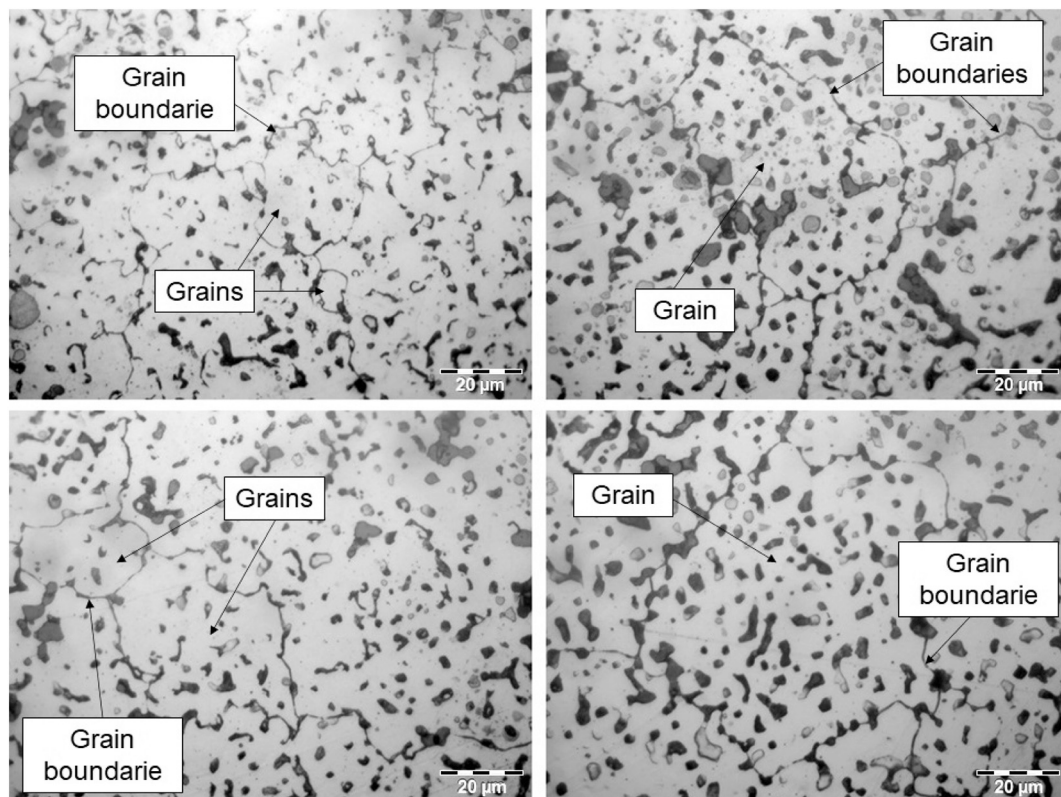


Fig. 4. Grain size. Metallography of sintered pure iron samples after etching 2% Nital.

**Table 2**  
Mechanical properties of pure iron samples obtained by MIM.

Sample	Yield strength (MPa)	Young's modulus (GPa)	Tensile strength (MPa)	Elongation (%)
1	86	113	236	35
2	65	128	312	42
3	96	132	328	53
4	67	138	334	48
Standard deviation	15.02	10.66	45.3	7.77
Average	78.5	127.75	302.5	44.5

Corrosion and degradation are also important aspects to be considered in the manufacture of iron. The density has an important role in this process and it needs to be evaluated in biodegradable implants [12]. Thus, we chose the metal injection molding (MIM) process because it allows the control of the porosity that will impact the density. MIM is a metal forming process by which finely-powdered metal is mixed with a binder material to comprise a “feedstock” capable of being handled by plastic processing equipment through a process known as injection molding [17]. The MIM process consists of 4 main steps (1) Mixing: Mixture of binder (polymer + waxes + acids) with the metallic powder to form a feedstock. (2) Injection molding: The feedstock is heated and provides the fluidity of the binder enabling the molding of the green part on an injection machine. (3) Debinding: The binder is removed from the green part and the remaining structure, now called the brown part, is constituted only of metallic powder. (4) Sintering: The metallic structure is heated and the union of metallic powders occurs through diffusion. In this step, the strength in the sintered part is achieved. MIM is characterized for its near net shaping technique that favors the development of complex shapes of high density, promoting great dimensional accuracy. In addition, this process can reduce production costs and allows large production quantities [18].

### MTT ASSAY 24h

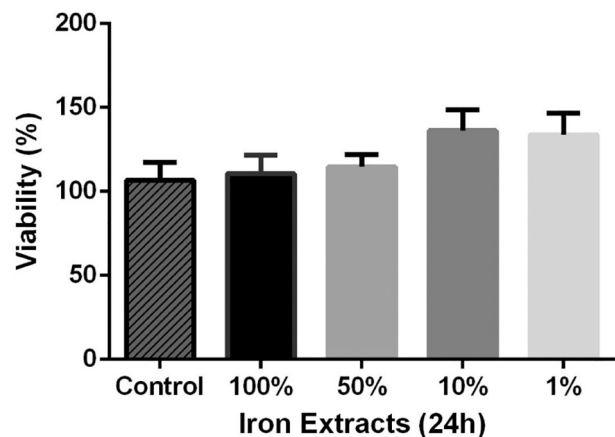


Fig. 5. Cell viability. Viability of ADSCs cultured for 24 h in iron extracts with 100%, 50% 10% and 1% concentration. Control: cells grown in DMEM Low Glucose. Values are means  $\pm$  SEM, N = 3. There is no statistically significant difference between groups.

The global powder injection molding industry has annual sales of approximately \$3 billion, as highlighted in recent applications in the field of micro-miniature medical devices and high added value [19]. MIM is appropriate for the manufacture of materials for medical applications such as stainless steel [20,21], titanium alloys [22], Co\Cr alloys [23], Bronze [24] as well as biodegradable metals such as zinc and magnesium alloys [25,26]. This process has been used in the healthcare industry for the manufacture of implants and biomedical devices, such as metallic orthodontic brackets, joint replacement surgery devices, medical equipment, and surgical instruments [27]. Iron has been

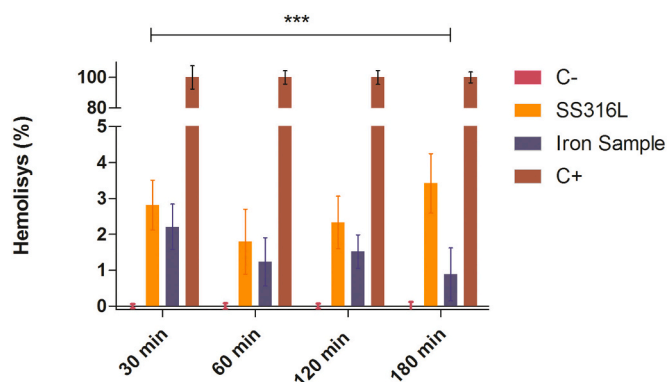


Fig. 6. Hemocompatibility. Hemolysis percentage in the presence of iron, using the SS316L as a golden standard. Negative control (C-): saline; Positive control (C+): distilled water, Values are means  $\pm$  SEM, N = 3 \*\*\*represents  $p < 0.001$ .

considered to be used in biomedical applications produced by MIM, but the studies are still scarce [28].

The choice of the cell type to assess the biocompatibility of the material *in vitro* is an important step for cytotoxicity evaluation. Mesenchymal stromal cells (MSCs) are an attractive option because they reside virtually in all tissues [29]. Moreover, they have potential to be used in the regenerative medicine field, in cell therapies, or associated with biomaterials [30,31] due to their immune-modulatory, anti-inflammatory, and angiogenic properties [32]. Among several sources of MSCs, adipose tissue has emerged as an attractive source because it contains an abundance of these cells and it is easier to obtain, allowing autologous transplantation [33].

Therefore, considering the advantages of metal injection molding technology and our previous results showing the better performance of 99.95% purity iron in comparison to 99.5% [6], we performed the first study that manufactured and evaluated the *in vitro* and *in vivo* biocompatibility of 99.95% iron samples, produced by MIM through a new eco-friendly feedstock from natural rubber (*Hevea brasiliensis*).

## 2. Materials and methods

### 2.1. Iron samples

The limits of the elements contained in the iron powder (Iyulong superfine metal Co., China) used in this research are Fe ( $\geq 99.95\%$ ), C ( $\leq 0.02\%$ ), S ( $\leq 0.01\%$ ), and O ( $\leq 0.02\%$ ). The 99.95% iron powder, D90 less than  $12 \mu\text{m}$  and average particle size of  $6 \mu\text{m}$ , was evaluated in a scanning electron microscope (Tescan Vega 3, Czech Republic). The material was used to produce samples by metal injection molding with

an eco-friendly feedstock containing 60 vol% iron powder. The binder was formulated with 57.5 wt% carnauba wax, 37.5 wt% natural rubber, and 5 wt% stearic acid and dicumyl peroxide. It was prepared according to described in the patent “BR 10 2013 008311-9 A2” [34].

Initially, the rheological test with the feedstock was carried out to obtain preliminary parameters for the metal injection molding process. All samples were injected with the shape of the tensile specimens in an injection molding machine (Thermo Scientific HAAKE MiniJet). The injectable parts, in this step known as green parts, were cut into flat squares with dimensions of approximately  $7.5 \times 7.5 \times 2.5 \text{ mm}$ . In the debinding step, a vacuum furnace (Sanchis, Brazil) was used, at a heating rate of  $0.1 \text{ }^\circ\text{C}/\text{min}$  up to a temperature of  $600 \text{ }^\circ\text{C}$  maintained for 60 min to remove possible traces of the binder. The remaining structures (brown parts) were constituted only of pure iron powder. After the debinding, the parts were sintered. The sintering step was performed in an electric tube furnace silicon carbide resistor (Sanchis, Brazil) with Argon gas-controlled atmosphere. The sintering cycle started at room temperature and heated up to  $1150 \text{ }^\circ\text{C}$  at a rate of  $10 \text{ }^\circ\text{C}/\text{min}$ . The temperature was maintained at  $1150 \text{ }^\circ\text{C}$  for 60 min to guarantee the complete sintering of the samples. After cooling, the parts followed for the physical, mechanical, and biocompatibility tests.

### 2.2. Physical and mechanical properties

In order to verify the physical properties of the samples, we measured the density of green and sintered parts according to MPIF 42 [35]. For these analyses, the masses of 15 samples were obtained by an analytical balance and the dimensions measured with a micrometer.

The metallographic test was performed to evaluate the morphology, grain size, and pores of the sintered samples. For this purpose, the specimens were mounted using a hot compression thermosetting resin. After mounting, the abrading process was started with aluminum oxide sandpaper of 100, 200, 400, 600, 800, 1000, and 1200 grit. At the end, samples were polished with alumina paste ( $1 \mu\text{m}$ ) [36] and subjected to etching by 2% Nital. Metallographic analyses were evaluated by optical microscopy (Olympus) before and after the etching process [37]. The measurement of grain size and pores was performed with the ImageJ software according to ASTM E 562-02 standard [37].

The mechanical properties were evaluated by Vickers microhardness, Brinell hardness, and tensile test. Vickers microhardness of 10 samples was determined by the Insize ISH-TDV 1000 durometer with a load of 0.5 kgf, according to ASTM E384 standard [38]. The Brinell hardness of 10 samples was determined by a hardness tester (MRS Fortel) using a 2.5 mm diameter indenter and a load of 62.5 kgf, according to ASTM E10 [39]. Finally, the tensile test of 4 samples was performed on a universal testing machine (Instron, Brazil) with a 50 kN load cell and speed of  $1 \text{ mm}/\text{min}$  at room temperature.

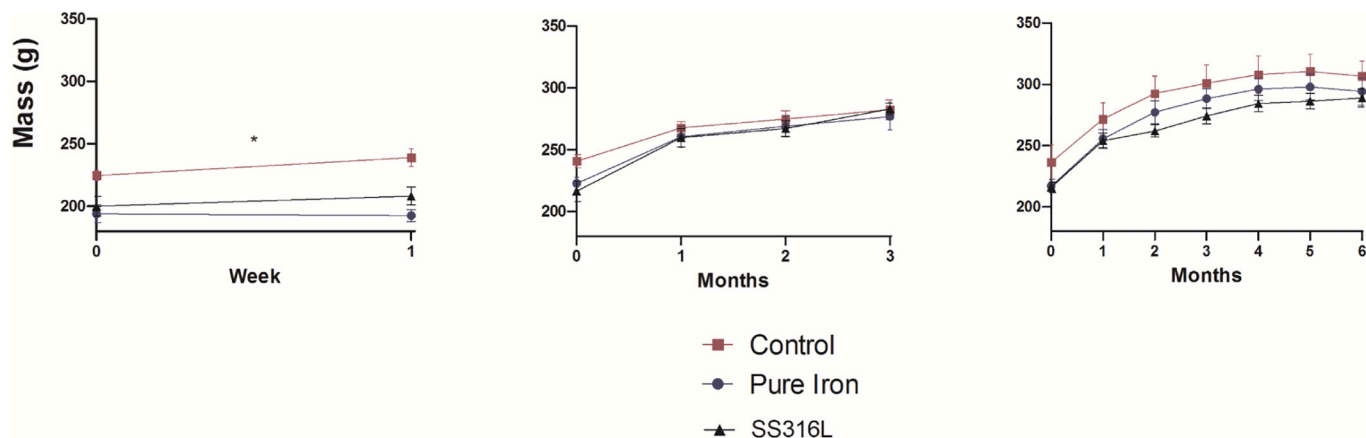
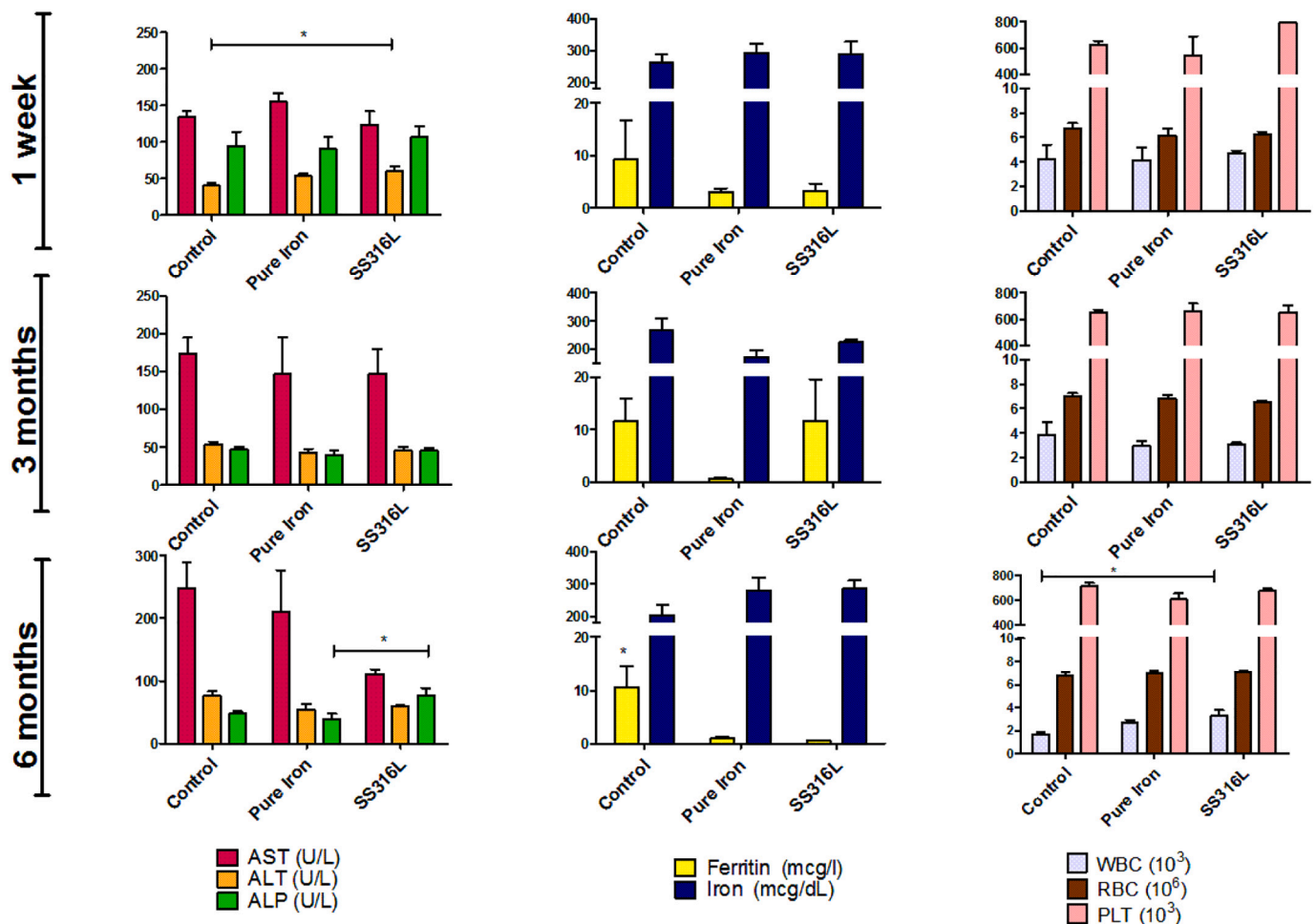


Fig. 7. Body weight. Change of Body Weight of animal groups after 1 week, 3 months and 6 months. Values are means  $\pm$  SEM \*represents  $p < 0.05$ .



**Fig. 8.** Blood and serum analysis after 1 week, 3 and 6 months of iron implantation. Control: sham group. Biochemical parameters: iron, ferritin, aspartate aminotransferase (AST), alanine aminotransferase (ALT) and alkaline phosphatase (ALP). Hematological parameters: red blood cell (RBC), white blood cell (WBC) and platelets (PLT) parameters. Values are means  $\pm$  SEM \*represents  $p < 0.05$ . (For interpretation of the references to colour in this figure legend, the reader is referred to the web version of this article.)

### 2.3. Indirect cytotoxicity assessment

#### 2.3.1. Adipose-derived stem cells: isolation and characterization

ADSCs were extracted from the abdominal adipose tissue of healthy adult donors during liposuction surgery. The study was conducted with approval from the Research Ethics Committee of Santa Casa de Misericórdia of Porto Alegre (REC-ISCMPA 3029.141) and the Research Ethics Committee of the Federal University of Health Sciences of Porto Alegre (REC-UFCSPA 3.734.612). The cells were isolated and characterized according to the protocol previously described by our research group [40,41].

#### 2.3.2. Indirect cytotoxicity testing (MTT assay)

Cell viability test was conducted by indirect method. For this experiment, the iron extract was prepared according to ISO 10993-5 and 10993-12. Samples were autoclaved and incubated with DMEM Low Glucose supplemented with 10% fetal bovine serum for 24 h under cell culture conditions (5%  $\text{CO}_2$ , 95% humidity, 37 °C) with a fixed mass ratio to medium volume (0.2 g/mL). The extracts were then collected without any filtration for cytotoxicity tests [42]. A colorimetric test (Bioclin® Kits, Brazil) was performed to evaluate the iron concentration in the extract.

ADSCs were pre-cultivated for 24 h at 37 °C, into 96-well plates at a ratio of  $3.0 \times 10^3$  cells per well. Next, the medium was removed and replaced by pure, 1:2, 1:10 and 1:100 dilutions of iron extract, and

incubated. As a control, ADSCs were incubated with a standard medium. The viability of the cells was tested after 24 h of incubation using MTT assay (3-(4,5-dimethylthiazol-2-yl)-2,5-diphenyltetrazolium bromide).

### 2.4. Hemolysis assay

Healthy human blood from volunteers containing sodium citrate (3.8 wt%) at a ratio of 9:1 was taken and diluted to 10 mL with PBS. The study was approved by the Research Ethics Committee of the Federal University of Health Sciences of Porto Alegre (REC-UFCSPA 3594.874). Pure iron and Stainless Steel (SS316L) specimens were dipped in separate standard tubes containing diluted erythrocytes and incubated for 30, 60, 120, and 180 min at 37 °C. As a positive control for hemolysis, blood was diluted in distilled water, whereas saline diluted blood was added to an empty standard tube which served as a negative control. After this period, specimens were removed and all the tubes were centrifuged at 3300 rpm for 5 min. The supernatant from each tube was transferred to a 96-well plate where the absorbance was measured with a microplate reader (SpectraMax) at 540 nm. Hemolysis was calculated as follows:

$$\text{Hemolysis (\%)} = \frac{(\text{OD sample} - \text{OD negative control})}{(\text{OD positive control} - \text{OD negative control})} \times 100$$

Where, OD means optical density.

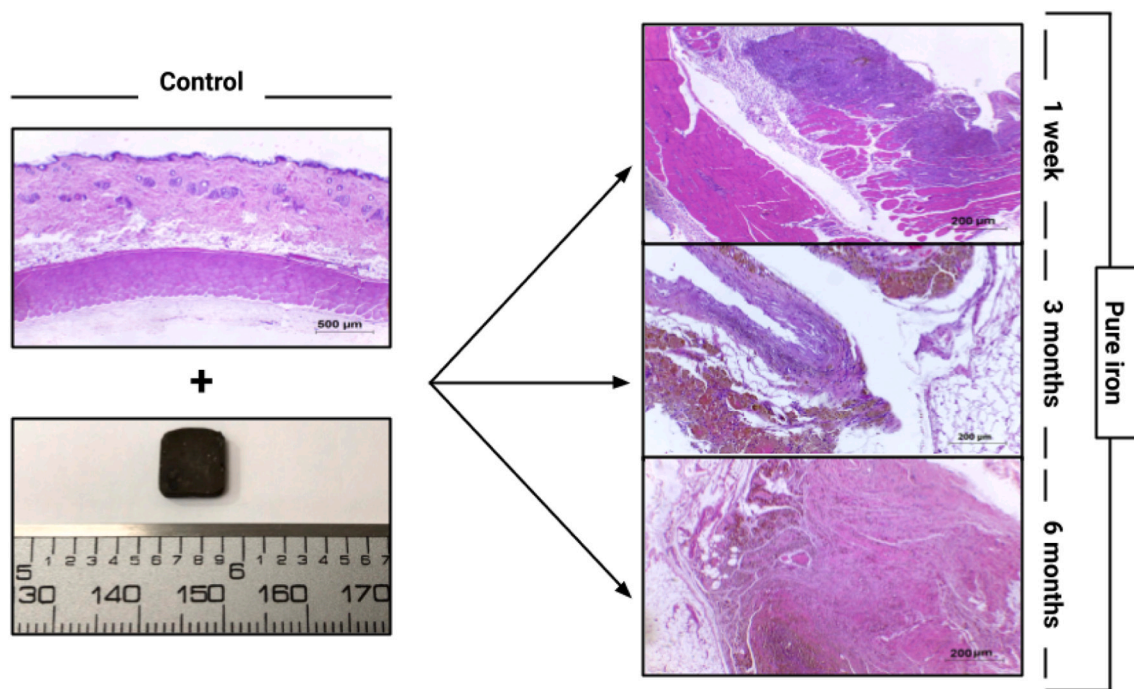


**Fig. 9.** Histological analysis of subcutaneous tissues located around the iron implants. Hematoxylin and eosin staining of the subcutaneous tissues at 1 week, 3 months and 6 months post-implantation.

### 2.5. *In vivo* study

*In vivo* biocompatibility of pure iron samples was evaluated after a subcutaneous implant in rats as previously described by our research group [6]. All animal procedures are in accordance with the National Council for Animal Experimentation Control and they were approved by UFCSPA Animal Ethics committee (613/19).

A total of 46 Wistar rats (171–262 g; mean: 219 g;  $\pm 8$  weeks) were randomized into the following 3 groups; pure iron implant; SS316L implant (one of the most common metals used for surgical implants) and sham control (without implant). Prior to surgery, the animals were anesthetized *via* intraperitoneal injection with an association of 90 mg/kg ketamine and 10 mg/kg xylazine. An incision was made through the cutaneous tissue in the dorsal region using a surgical scissor. The pure iron or SS316L implant was inserted into this opening, after which the skin was sutured. The sham control group received the same surgical procedure but no implant.

Tramadol Hydrochloride (5 mg/kg) was administered subcutaneously on rats to provide pain relief. The animals were monitored daily during the first two weeks for surgical wound appearance, locomotion in their cage, and general well-being. The body mass of each rat was monitored monthly during the study.

After 2 weeks, 3 months, and 6 months, one third of the rats in each group was euthanized by cardiac puncture preceded by general anesthesia with 90 mg/kg ketamine and 10 mg/kg xylazine, followed by implant and tissue harvest. Blood was collected in EDTA for complete blood cell, red blood cell (RBC) and white blood cell (WBC) counts and for determining platelets (PLT) levels. The analyzes of non-coagulated blood samples were performed in the BC-5380 auto hematology analyzer (Mindray, Shenzhen, China).

The levels of serum biochemical parameters- iron, ferritin, aspartate aminotransferase (AST), alanine aminotransferase (ALT), and alkaline phosphatase (ALP)- were also assessed using diagnostic kits (Bioclin® Kits, Brazil) in the BS-120 chemistry analyzer (Mindray, Shenzhen, China).

To evaluate the impact of pure iron implants, the tissue around the samples and organs were histologically analyzed. The collected samples

were preserved in a 10% buffered formaldehyde solution. After this step, they were trimmed, paraffin embedding, sectioned to a thickness of 4 mm and deparaffinized on microscopy slides. So, tissue samples were stained with hematoxylin and eosin (H&E) and assessed by a veterinary pathologist to identify histological changes.

The degradation study included visual examination, ultrasonication, cleaning, and weighing of the extracted implants to determine the mass variation.

### 2.6. Statistical analysis

Data samples were statistically compared by *t*-test and ANOVA using GraphPad Prism biostatistics software (GraphPad Inc., USA). Differences between mean values were considered significant when  $p < 0.05$ .

## 3. Results

### 3.1. Feedstock characteristic analysis

Scanning electron microscope (SEM) images of the 99.95% iron powder used in the manufacture of the feedstock were obtained. Fig. 1 presents the images of iron powder, where it is possible to verify spherical shape powder and particle size varying from 1 to 5  $\mu\text{m}$ .

After mixing the eco-friendly feedstock, the rheological test was carried out to check preliminary parameters for setting the injection process. The rheology shear rates were indicated by the capillary rheometer manufacturer due to the high rates that the injection process uses [44]. Fig. 2 shows the results of rheology at temperatures of 120 °C, 125 °C, and 130 °C, within the working range of this eco-friendly feedstock.

Based on the results presented in Fig. 2 and knowing that the injection process uses high shear rates, the temperature range between 120 °C to 130 °C is suitable for the process. It was chosen to use the injection temperature of 120 °C to manufacture the samples since the energy consumption of the equipment is lower. The rheological results obtained at 120 °C are shown in Table 1.

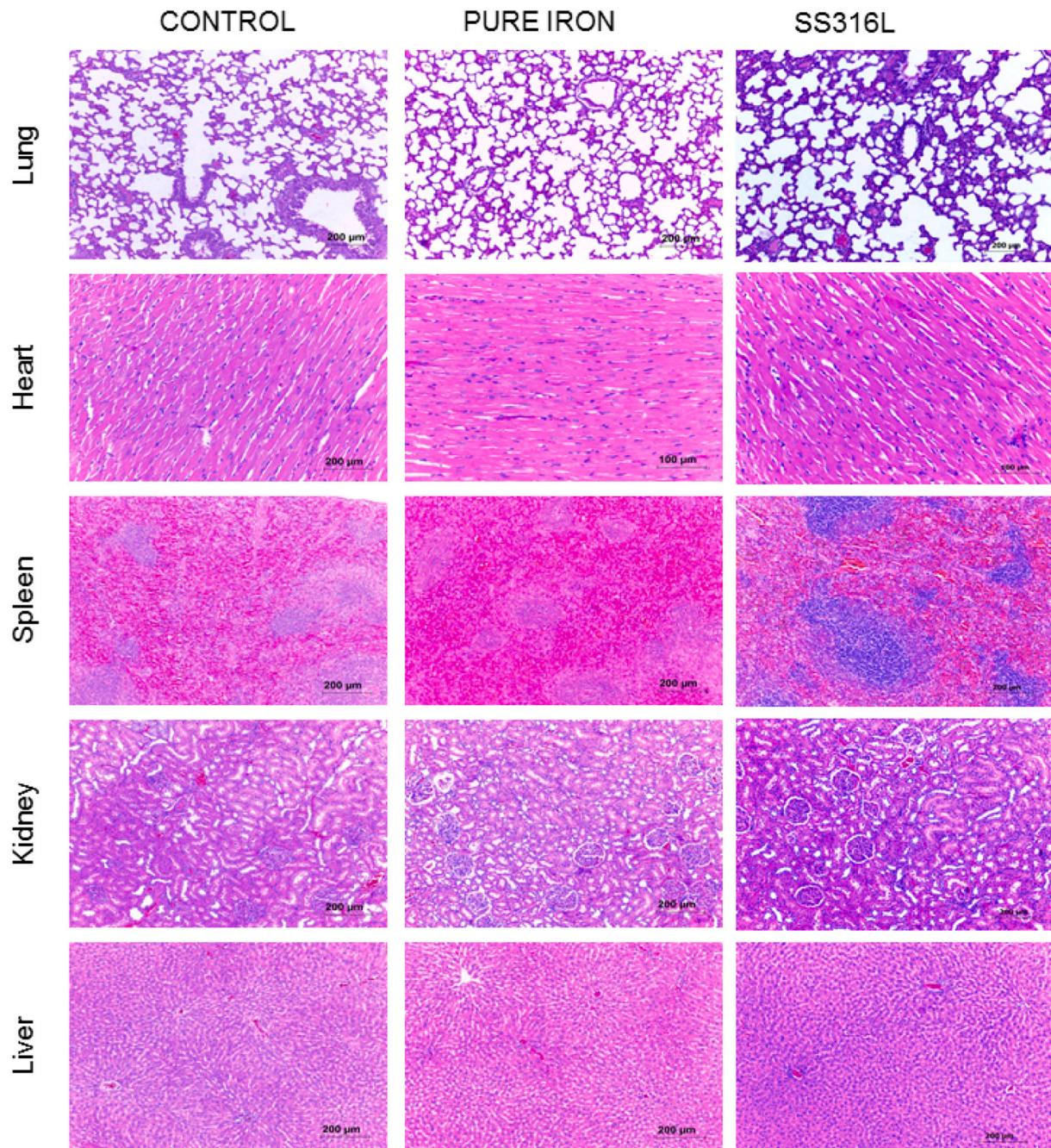


**Fig. 10.** Histological analysis of the major organs. Hematoxylin and eosin staining of the main organs of rats (lung, heart, kidney, spleen and liver) after 6 months of iron and SS316L implantation in the subcutaneous tissue. Control: sham group.

**Table 3**

Masses of pure iron samples before and after implantation in the subcutaneous tissue of Wistar rats using paired t-test.

	Pure iron implant			
	N	Average pre implantation (g)	Average post implantation (g)	P-value
1 week	6	1.199 ± 0.068	1.207 ± 0.070	p < 0.05
3 Months	6	1.267 ± 0.108	1.298 ± 0.108	p < 0.05
6 Months	5	1.143 ± 0.025	1.202 ± 0.045	0.064

### 3.2. Physical and mechanical properties of iron samples obtained by MIM

The 99.95% iron injected samples showed a green density of 4.96 g/cm<sup>3</sup> ± 0.16, exhibiting repeatability and stability of mass and volume in

the MIM process. After debinding and sintering steps, the samples showed sintered density of 6.61 g/cm<sup>3</sup> ± 0.12.

Metallographic testing was performed to determine the porosity and grain size of the sintered samples. Fig. 3 shows the metallography of the

samples without etching. It is possible to observe that the pores measured between 0.8 and 11.7  $\mu\text{m}$  (average size of 1.5  $\mu\text{m} \pm 1$ ).

The microstructural grains can be observed in Fig. 4 that shows a sintered pure iron sample after etching with 2% Nital. The samples have grains with 45.14  $\mu\text{m} \pm 23.20$ , showing a large variation in size.

The Vickers microhardness on the sintered pure iron samples showed heterogeneity in the measured values, ranging from 57.6 to 77.2 HV, with an average of 61.5 HV. The Brinell hardness values were homogeneous and the samples showed 69.1 HB  $\pm 4.8$ .

Table 2 shows the results of the tension test of the pure iron samples obtained by the MIM process.

### 3.3. ADSCs differentiation

MSCs were initially tested for tri-lineage differentiation and expression of MSC surface markers (Supp. Fig. 1). They exhibited osteogenic potential, as demonstrated by marked staining with alizarin red S, adipogenic potential characterized by a higher number of adipocytes stained by oil red O and chondrogenic potential, as evidenced by alcian blue staining. As previously published by our group [6], flow cytometry results showed that the isolated cells expressed CD44, CD105, CD90, and CD73 and they are negative for hematopoietic markers CD14, CD34, and CD45. These results indicate that ADSCs were successfully isolated.

### 3.4. Viability assay

Fig. 5 shows the relative viabilities of ADSCs cultured in extracts from the pure iron in relation to the negative control (DMEM-Low glucose), after incubation for 1 day. Pure iron extracts maintained the cell viability, morphology and adherence to plastic in comparison with control. The colorimetric test showed that the iron concentration in the extract is 1645  $\mu\text{g}/\text{dL} \pm 75$  (N = 2).

### 3.5. In vitro hemocompatibility

The hemolysis percentage of experimental pure iron and stainless steel 316 L samples is shown in Fig. 6. Iron samples did not exhibit hemolytic activity under the conditions used in this study. The hemolysis ratio of samples tested in the time frame of 30 to 180 min was lower than 5%. Thus, they can be categorized as hemocompatible, according to ASTM-F756-08 [45].

### 3.6. In vivo biocompatibility

Post-implantation mass gain by rats with iron implants is shown in Fig. 7. All rats with implants gained mass at the same rate that the sham control and SS316L groups. In addition, there were no important alterations in the hematological (RBC, WBC, and PLT) and biochemical parameters (Fe, ferritin, AST, ALT, and ALP) evaluated between the groups (Fig. 8).

The histological analysis of the subcutaneous tissues showed a fibrous encapsulation of implanted material and the presence of macrophages with intracytoplasmic granules of brown pigment. However, there was no evidence of inflammation or necrosis in the subcutaneous tissues located close to the iron implants (Fig. 9). As expected, SS316L also did not cause inflammation or necrosis in the animals (Supp. Fig. 2).

Cells of the lung, kidney, heart and liver also did not present histological changes up to 6 months after the iron implantation in comparison to sham control and SS316L groups (Fig. 10). The iron implants did not show relevant signs of corrosion after 1 week, 3 or 6 months in the subcutaneous tissue of the animals (Table 3).

## 4. Discussion

Powder metallurgy technology, in specific the MIM, has been recognized as one of the prominent methods to produce components for

different fields and industries. Additionally, this technique has also been employed in the medical field for fabricating implants used in surgery and dentistry [18,46]. However, there are only a few studies using pure iron in the production of MIM to biomedical devices. Therefore, in this study we produced pure iron samples by MIM, employing an eco-friendly feedstock extracted from *Hevea brasiliensis*.

The main characteristic of this innovation is the elastic properties of the natural rubber feedstock due to the flexibility of the polymer chains, as well as the restriction to permanent deformation. The elastic factor is an advantage for removing the injected part from the die without compromising its structure. Therefore, natural rubber is a promising alternative to be used as a binder in feedstocks for medical devices and other complex geometry parts.

It is important to highlight that the temperatures for working with natural rubber in the MIM process are different from those used in thermoplastic materials since the crosslinking of natural rubber is temperature-dependent. Because of this, the iron samples show a pseudo-plastic behavior that is essential for the MIM process [47]. We also evaluated the physical and mechanical properties, as well as the *in vitro* and *in vivo* biocompatibility of injected iron samples.

The physical properties evaluated were powder morphology, density, porosity and microstructural grain size. SEM images of the iron powder demonstrated a material of spherical morphology due to the atomization process. Particles less than 10  $\mu\text{m}$  and with different distribution sizes become the iron, a suitable feature for use in the injection process [48,49]. The samples showed homogeneous green density variation, ensuring the repeatability and stability of the injection process.

The density of the sintered parts obtained by MIM reached 83.9% of the relative density of the iron, so the average porosity percentage was approximately 16%, in accordance with other studies [28]. In the metallographic analysis, small pores were found. It is necessary to emphasize that porosity is an important feature for a bioabsorbable material, as it would enable a higher rate of corrosion, absorption and facilitate the adhesion of drugs [50]. In addition, samples presented varied grain sizes, a characteristic that results in mechanical properties suitable for medical applications [51].

The mechanical properties of the samples were evaluated by Vickers microhardness, Brinell hardness, and tensile tests. The microhardness of the samples showed heterogeneous values with a range of 31.86% in relation to the average because of high porosity, while Brinell hardness showed low variation ( $\pm 4.8$  HB) indicating that the dispersion of the pores is homogeneous in the sample.

These hardness results are equivalent to those found in biomedical magnesium alloys applied *in vivo* studies [52]. The tensile test showed variation in the maximum displaced tensions, due to the porosity. It is important to note that the elastic deformation in porous materials is different from solid materials [28,53,54]. The tensile test presented the yield strength between 65 MPa and 96 MPa and elongation between 35% and 53%. Specialized literature shows that elongation between 30 and 50% is adequate, for example, to withstand the balloon inflation process, when applied to stents [55,56]. Our results exhibited strengths values between the SS316L and magnesium alloys and high ductility, a required property for cardiovascular materials [27,53,57].

Pure iron samples processed by MIM and by casting were compared. It was found that the porosity retained in the sintered samples has a major effect on the mechanical properties than casting samples [28,53,54]. In addition, it is possible to state that several materials applicable to medical devices have different mechanical behavior. Thus, the results presented in this article are in accordance with values found in the literature [57–59].

Based on the results of the *in vitro* biocompatibility tests, pure iron samples obtained by MIM are biocompatible with ADSCs and hemocompatible. ADSCs did not alter their viability, morphology and adherence to plastic, after iron extract exposition, indicating that they remained viable. The material is considered cytotoxic, according to ISO

10993-5, if cell viability is reduced by more than 30%. Thus, pure iron can be considered compatible with ADSCs [60]. In accordance with our results, Imgrund et al. (2013) produced biodegradable iron-based materials by MIM and characterized its biocompatibility, mechanical and degradation properties. Extracts of Fe and Fe-0.6P samples showed good cytocompatibility after 24 h independent of the sintering conditions [61].

The hemolysis percentage promoted by the pure iron samples produced by MIM was lower than 5%, therefore they can be categorized as hemocompatible. These results are in line with other studies, which found that pure Fe shows adequate cytocompatibility [11,62,63] and good hemocompatibility [63–66].

*In vivo* assessment of rats containing pure iron implants in respect of well-being, biochemical, hematological and histological analysis of organs were in order with results obtained by the SS316L and control groups, as well as other published studies [6,43]. Animals did not show significant alteration over the follow-up months in weight gain, serum biochemical and hematological parameters in comparison to SS316L and control groups. The histopathological analyses showed that iron implants were not toxic to major organs. Macrophages were observed in the capsule formed around the iron implant, but it was already expected, considering that they are among the first cells to react to any tissue injury or introduced foreign material, such as implants [67,68]. *In vivo* degradation tests of pure iron have shown a rather low biodegradation rate in different studies, a characteristic also found by us [4,69].

## 5. Conclusions

In this study, pure iron was manufactured by metal injection molding with the new eco-friendly feedstock. We presented that the mechanical and physical properties evaluated, density, microhardness, hardness, yield strength and stretching, are suitable for biomedical devices.

We also showed that the iron samples are biocompatible *in vitro* and *in vivo*. The pure iron samples were cytocompatible with ADSCs, hemocompatible and they did not promote toxicity *in vivo* after subcutaneous implantation in Wistar rats. Therefore, pure iron produced by MIM can be considered a promising material for biomedical applications.

Supplementary data to this article can be found online at <https://doi.org/10.1016/j.msec.2021.112532>.

## Founding

This study was financed in part by the Coordenação de Aperfeiçoamento de Pessoal de Nível Superior – Brasil (CAPES) – Finance Code 001; FAPERGS/MS/CNPq/SESRS n. 03/2017 – PPSUS 17/2551-0001 (Process: 416-2, Marcia R. Wink and 413-8, Lírio Schaeffer); FAPERGS/CNPq/SEBRAE 08/2019 - PDEmp 20/2551-0000207-1 (Diego P. Wermuth) and CNPq MS-SCTIE-Decit/CNPq n° 12/2018 (441575/2018-8).

Thaís Casagrande Paim, Mônica Slaviero and Liliana Ivete Sous Naasani are recipients of fellowships from the Coordenação de Aperfeiçoamento de Pessoal de Nível Superior (CAPES). Diego Pacheco Wermuth is recipient from the Fundação de Amparo à Pesquisa do Estado do Rio Grande do Sul (FAPERGS), Isadora Bertaco and Carla Zanatelli are recipients from Conselho Nacional de Desenvolvimento Científico e Tecnológico (CNPq). Márcia Rosângela Wink, Lírio Schaeffer, Luis Alberto Loureiro dos Santos and David Driemeier are recipients of a research productivity fellowship from the CNPq.

## CRedit authorship contribution statement

**Diego Pacheco Wermuth:** Conceptualization, Data curation, Formal analysis, Methodology; Investigation; Visualization; Funding acquisition; Engineering project administration; Roles/Writing - original draft; Writing - review & editing.

**Thaís Casagrande Paim:** Conceptualization, Data curation, Formal

analysis, Methodology; Investigation; Visualization; Funding acquisition; Roles/Writing - original draft; Writing - review & editing.

**Isadora Bertaco dos Santos:** Investigation; Validation; Visualization.

**Carla Zanatelli:** Conceptualization; Investigation.

**Liliana Ivete Sous Naasani:** Conceptualization; Investigation.

**Mônica Slaviero:** Pathological investigation and its formal analysis.

**David Driemeier:** Pathological investigation and its formal analysis.

**André Carvalho Tavares:** Engineering formal analysis.

**Vinicius Martins:** Engineering formal analysis.

**Camila Ferreira Escobar:** Conceptualization of engineering, Formal analysis, Visualization; Investigation; Validation.

**Luis Alberto Loureiro dos Santos:** Conceptualization of engineering Resources; Supervision.

**Lirio Schaeffer:** Conceptualization; Funding acquisition; Project administration; Resources; Engineering supervision.

**Márcia Rosângela Wink:** Conceptualization, Formal analysis; Methodology; Funding acquisition; Project administration; Resources; Cell biology supervision; Roles/Writing - original draft; Writing - review & editing.

## Declaration of competing interest

The authors declare that they have no known competing financial interests or personal relationships that could have appeared to influence the work reported in this paper.

## Acknowledgments

The authors would like to thank Giuliano Rizzotto Guimarães and Terezinha Stein (Laboratório de Pesquisa em Patologia, UFCSPA), Laura Alencastro de Azevedo (Laboratório de Análises Clínicas, UFCSPA), Laura Alencastro de Azevedo (Laboratório de Análises Clínicas e Toxicológicas, UFRGS) and André Rosiak (Laboratório de Transformação Mecânica, UFRGS) for excellent technical support. The authors also gratefully acknowledge both veterinary physicians Dr. Joana Fisch and Dr. Fernanda Bastos de Mello for their assistance in the UFCSPA Animal facility.

## References

- [1] F. Mahyudin, H. Hermawan, *Biomaterials and Medical Devices: A Perspective From an Emerging Country*, Springer, 2016.
- [2] M. Prakasam, J. Locs, K. Salma-Ancane, D. Loca, A. Largeteau, L. Berzina-Cimdina, Biodegradable materials and metallic implants-a review, *J. Funct. Biomater.* 8 (2017), <https://doi.org/10.3390/jfb8040044>.
- [3] H. Ryu, M.-H. Seo, J.A. Rogers, Bioresorbable metals for biomedical applications: from mechanical components to electronic devices, *Adv. Healthc. Mater.* 10 (17) (2021), e2002236, <https://doi.org/10.1002/adhm.202002236>.
- [4] M. Peuster, C. Hesse, T. Schloo, C. Fink, P. Beerbaum, C. von Schnakenburg, Long-term biocompatibility of a corrodible peripheral iron stent in the porcine descending aorta, *Biomaterials* 27 (2006) 4955–4962.
- [5] M. Peuster, P. Wohlsein, M. Brüggemann, M. Eherding, K. Seidler, C. Fink, H. Brauer, A. Fischer, G. Hausdorf, A novel approach to temporary stenting: degradable cardiovascular stents produced from corrodible metal-results 6–18 months after implantation into New Zealand white rabbits, *Heart* 86 (2001) 563–569.
- [6] T.C. Paim, D.P. Wermuth, I.B. dos Santos, C. Zanatelli, L.I.S. Naasani, M. Slaviero, D. Driemeier, L. Schaeffer, M.R. Wink, Evaluation of *in vitro* and *in vivo* biocompatibility of iron produced by powder metallurgy, *Mater. Sci. Eng. C* 115 (2020), 111129.
- [7] S. Garg, P.W. Serruys, Coronary stents: looking forward, *J. Am. Coll. Cardiol.* 56 (2010) S43–S78.
- [8] R. Waksman, R. Pakala, R. Baffour, R. Seabron, D. Hellinga, F.O. Tio, Short-term effects of biocorrodible iron stents in porcine coronary arteries, *J. Interv. Cardiol.* 21 (2008) 15–20.
- [9] G. Mani, M.D. Feldman, D. Patel, C.M. Agrawal, Coronary stents: a materials perspective, *Biomaterials* 28 (2007) 1689–1710.
- [10] L. Zema, G. Loreti, A. Melocchi, A. Maroni, A. Gazzaniga, Injection molding and its application to drug delivery, *J. Control. Release* 159 (2012) 324–331.
- [11] H. Hermawan, A. Purnama, D. Dube, J. Couet, D. Mantovani, Fe–Mn alloys for metallic biodegradable stents: degradation and cell viability studies, *Acta Biomater.* 6 (2010) 1852–1860, <https://doi.org/10.1016/j.actbio.2009.11.025>.

- [12] M. Moravej, A. Purnama, M. Fiset, J. Couet, D. Mantovani, Electroformed pure iron as a new biomaterial for degradable stents: in vitro degradation and preliminary cell viability studies, *Acta Biomater.* 6 (2010) 1843–1851.
- [13] G. Gašior, J. Szczepański, A. Radtke, Biodegradable iron-based materials—what was done and what more can be done? *Materials* 14 (2021) 3381, <https://doi.org/10.3390/ma14123381>.
- [14] Z. Luo, X. Zhuang, D. Kumar, X. Wu, C. Yue, C. Han, J. Lv, The correlation of hippocampal T2-mapping with neuropsychology test in patients with Alzheimer's disease, *PLoS One* 8 (2013), e76203.
- [15] S. Aytton, A. Fazlollahi, P. Bourgeat, P. Raniga, A. Ng, Y.Y. Lim, I. Diouf, S. Farquharson, J. Fripp, D. Ames, J. Doecke, P. Desmond, R. Ordidge, C.L. Masters, C.C. Rowe, P. Maruff, V.L. Villemagne, Australian Imaging Biomarkers and Lifestyle (AIBL) Research Group, O. Salvado, A.I. Bush, Cerebral quantitative susceptibility mapping predicts amyloid- $\beta$ -related cognitive decline, *Brain* 140 (2017) 2112–2119.
- [16] Y. Kohgo, K. Ikuta, T. Ohtake, Y. Torimoto, J. Kato, Body iron metabolism and pathophysiology of iron overload, *Int. J. Hematol.* 88 (2008) 7–15.
- [17] R.M. German, Metal powder injection molding (MIM): key trends and markets, in: *Handbook of Metal Injection Molding*, Elsevier, 2012, pp. 1–25.
- [18] M.F.F.A. Hamidi, W.S.W. Harun, M. Samykano, S.A.C. Ghani, Z. Ghazalli, F. Ahmad, A.B. Sulong, A review of biocompatible metal injection moulding process parameters for biomedical applications, *Mater. Sci. Eng. C Mater. Biol. Appl.* 78 (2017) 1263–1276.
- [19] Professor German updates his views on the present and future outlook for powder injection molding, *Met. Powder Rep.* 74 (2019) 118–120.
- [20] S.-H. Zhu, G.-H. Wang, Y.-Z. Zhao, Y.-M. Li, K.-C. Zhou, B.-Y. Huang, Biocompatibility of MIM 316L stainless steel, *J. Cent. S. Univ. Technol.* 12 (2005) 9–11, <https://doi.org/10.1007/s11771-005-0362-9>.
- [21] H.O. Gulsoy, H. Ozkan Gulsoy, S. Pazarlioglu, N. Gulsoy, B. Gundede, O. Mutlu, Effect of zr, nb and ti addition on injection molded 316L stainless steel for bio-applications: mechanical, electrochemical and biocompatibility properties, *J. Mech. Behav. Biomed. Mater.* 51 (2015) 215–224, <https://doi.org/10.1016/j.jmbm.2015.07.016>.
- [22] A. Dehghan-Manshadi, M.J. Birmingham, M.S. Dargusch, D.H. StJohn, M. Qian, Metal injection moulding of titanium and titanium alloys: challenges and recent development, *Powder Technol.* 319 (2017) 289–301, <https://doi.org/10.1016/j.powtec.2017.06.053>.
- [23] G. Herranz, C. Berges, J.A. Naranjo, C. García, I. Garrido, Mechanical performance, corrosion and tribological evaluation of a co-cr-mo alloy processed by MIM for biomedical applications, *J. Mech. Behav. Biomed. Mater.* 105 (2020), 103706.
- [24] K.A. Chun, K.-Y. Kum, W.-C. Lee, S.-H. Baek, H.-W. Choi, W.-J. Shon, Evaluation of the safety and efficiency of novel metallic implant scaler tips manufactured by the powder injection molding technique, *BMC Oral Health* 17 (2017) 110.
- [25] M. Wolff, J.G. Schaper, M.R. Suckert, M. Dahms, T. Ebel, R. Willumeit-Römer, T. Klassen, Magnesium powder injection molding (MIM) of orthopedic implants for biomedical applications, *JOM* 68 (2016) 1191–1197, <https://doi.org/10.1007/s11837-016-1837-x>.
- [26] X. Luo, C. Fang, Z. Fan, B. Huang, J. Yang, Semi-solid powder moulding for preparing medical Mg–Zn alloy, microstructure evolution and mechanical properties, *Mater. Res. Express* 6 (2019), 076528, <https://doi.org/10.1088/2053-1591/ab14b0>.
- [27] A. Dehghan-Manshadi, P. Yu, M. Dargusch, D. StJohn, M. Qian, Metal injection moulding of surgical tools, biomaterials and medical devices: a review, *Powder Technol.* 364 (2020) 189–204, <https://doi.org/10.1016/j.powtec.2020.01.073>.
- [28] P. Mariot, M.A. Leeftang, L. Schaeffer, J. Zhou, An investigation on the properties of injection-molded pure iron potentially for biodegradable stent application, *Powder Technol.* 294 (2016) 226–235, <https://doi.org/10.1016/j.powtec.2016.02.042>.
- [29] L. da Silva Meirelles, P.C. Chagastelles, N.B. Nardi, Mesenchymal stem cells reside in virtually all post-natal organs and tissues, *J. Cell Sci.* 119 (2006) 2204–2213.
- [30] L. Mazini, L. Rochette, M. Amine, G. Malka, Regenerative capacity of adipose derived stem cells (ADSCs), comparison with mesenchymal stem cells (MSCs), *Int. J. Mol. Sci.* 20 (2019), <https://doi.org/10.3390/ijms20102523>.
- [31] T. Montero-Vilchez, A. Sierra-Sánchez, M. Sanchez-Diaz, M.I. Quiñones-Vico, R. Sanabria-de-la-Torre, A. Martínez-Lopez, S. Arias-Santiago, Mesenchymal stromal cell-conditioned medium for skin diseases: a systematic review, *Front. Cell Dev. Biol.* 9 (2021), 654210.
- [32] C. Chang, J. Yan, Z. Yao, C. Zhang, X. Li, H.-Q. Mao, Effects of mesenchymal stem cell-derived paracrine signals and their delivery strategies, *Adv. Healthc. Mater.* 10 (2021), e2001689.
- [33] L. Mazini, M. Ezzoubi, G. Malka, Overview of current adipose-derived stem cell (ADSCs) processing involved in therapeutic advancements: flow chart and regulation updates before and after COVID-19, *Stem Cell Res Ther* 12 (2021) 1.
- [34] Escobar, Processo de obtenção de ligante “binder” baseado em poli (isopreno) utilizado na moldagem de pós por injeção (mpi) e uso, BR 10 2013 008311-9 A2, 2013.
- [35] Metal Powder Industries Federation, Standard Test Method 42: Method for Determination of Density of Compacted or Sintered Powder Metallurgy (PM) Products Materials, Princeton, 2016.
- [36] E04 Committee, Guide for Preparation of Metallographic Specimens, ASTM International, West Conshohocken, PA, 2017, <https://doi.org/10.1520/E0003-11R17>.
- [37] E04 Committee, Test Method for Determining Volume Fraction by Systematic Manual Point Count, ASTM International, West Conshohocken, PA, 2019, <https://doi.org/10.1520/E0562-19>.
- [38] E04 Committee, Test Method for Microindentation Hardness of Materials, ASTM International, West Conshohocken, PA, 2017, <https://doi.org/10.1520/E0384-17>.
- [39] E28 Committee, Test Method for Brinell Hardness of Metallic Materials, ASTM International, West Conshohocken, PA, 2015, <https://doi.org/10.1520/E0010-15>.
- [40] L.I.S. Naasani, A.F.D. Souza, C. Rodrigues, S. Vedovatto, J.G. Azevedo, A.P. S. Bertoni, M. Da Cruz Fernandes, S. Buchner, M.R. Wink, Decellularized human amniotic membrane associated with adipose derived mesenchymal stromal cells as a bioscaffold: physical, histological and molecular analysis, *Biochem. Eng. J.* 152 (2019), 107366, <https://doi.org/10.1016/j.bej.2019.107366>.
- [41] S. Vedovatto, J.C. Facchini, R.K. Batista, T.C. Paim, M.I.Z. Lionzo, M.R. Wink, Development of chitosan, gelatin and liposome film and analysis of its biocompatibility in vitro, *Int. J. Biol. Macromol.* 160 (2020) 750–757.
- [42] International Organization for Standardization, ISO 10993-12:2012 Biological Evaluation of Medical Devices — Part 12: Sample Preparation and Reference Materials, 2012.
- [43] A. Drynda, T. Hassel, F.W. Bach, M. Peuster, In vitro and in vivo corrosion properties of new iron-manganese alloys designed for cardiovascular applications, *J Biomed Mater Res B Appl Biomater* 103 (2015) 649–660.
- [44] R.M. German, Powder Injection Molding, German Metal Powder Industries Federation American Powder Metallurgy, Princeton, 1990.
- [45] ASTM International, Standard Practice for Assessment of Hemolytic Properties of Materials, West Conshohocken, PA, 2008, <https://doi.org/10.1520/f0756-08>.
- [46] S. Supriadi, D. Abdussalam, T. Heriyanto, B. Irawan, B. Suharno, Transformation of orthodontics bracket geometry in metal injection molding process, *IOP Conf. Ser. Mater. Sci. Eng.* 432 (2018), 012002, <https://doi.org/10.1088/1757-899x/432/1/012002>.
- [47] R.M. German, A. Bose, Injection Molding of Metals and Ceramics, Metal Powder Industry, 1997.
- [48] P.A. Davies, G.R. Dunstan, D.F. Heaney, T.J. Mueller, Comparison of master alloy and pre-alloyed 316L stainless steel powders for metal injection molding (MIM), in: *PM2 TEC 2004 World Congress*, Chicago, 2004. [https://www.materials.sandvik/globalassets/global/downloads/products\\_downloads/metal\\_powders/technical\\_papers/comparison-of-master-alloy-and-pre-alloyed-316L.pdf](https://www.materials.sandvik/globalassets/global/downloads/products_downloads/metal_powders/technical_papers/comparison-of-master-alloy-and-pre-alloyed-316L.pdf).
- [49] R.M. German, Powder Metallurgy Science, Metal Powder Industries Federation, Princeton, 1994.
- [50] J.J. Elsner, A. Kraitzer, O. Grinberg, M. Zilberman, Highly porous drug-eluting structures: from wound dressings to stents and scaffolds for tissue regeneration, *Biomater* 2 (2012) 239–270.
- [51] N. Baltzer, T. Coppnax, Precious Metals for Biomedical Applications, Elsevier, 2014.
- [52] X. Gu, W.R. Zhou, Y. Zheng, Y. Cheng, S. Wei, S.P. Zhong, T.F. Xi, L.J. Chen, Corrosion fatigue behaviors of two biomedical mg alloys – AZ91D and WE43 – in simulated body fluid, *Acta Biomater.* 6 (2010) 4605–4613.
- [53] P.K. Bowen, J. Drelich, J. Goldman, A new in vitro-in vivo correlation for bioabsorbable magnesium stents from mechanical behavior, *Mater. Sci. Eng. C* 33 (2013) 5064–5070, <https://doi.org/10.1016/j.msec.2013.08.042>.
- [54] B. Song, S. Dong, S. Deng, H. Liao, C. Coddet, Microstructure and tensile properties of iron parts fabricated by selective laser melting, *Opt. Laser Technol.* 56 (2014) 451–460, <https://doi.org/10.1016/j.optlastec.2013.09.017>.
- [55] K. Patatas, G. Robinson, V. Shrivastava, R. Lakshminarayan, A novel endovascular technique in the management of a large internal iliac artery aneurysm associated with an arteriovenous fistula, *Cardiovasc. Revasc. Med.* 14 (2013) 62–65, <https://doi.org/10.1016/j.carrev.2012.10.002>.
- [56] A. Witkowski, W. Ruzylto, R. Gil, B. Górecka, Z. Purzycki, M. Kośmider, L. Poloński, A. Lekston, M. Gasior, K. Zmudka, P. Pieniązek, P. Buszman, J. Drzewiecki, D. Ciećwierz, Z. Sadowski, A randomized comparison of elective high-pressure stenting with balloon angioplasty: six-month angiographic and two-year clinical follow-up. On behalf of AS (Angioplasty or Stent) trial investigators, *Am. Heart J.* 140 (2000) 264–271.
- [57] B. Al-Mangour, R. Mongrain, S. Yue, Coronary stents fracture: an engineering approach (review), *Mater. Sci. Appl.* 04 (2013) 606–621, <https://doi.org/10.4236/msa.2013.410075>.
- [58] M. Moravej, D. Mantovani, Biodegradable metals for cardiovascular stent application: interests and new opportunities, *Int. J. Mol. Sci.* 12 (2011) 4250–4270.
- [59] H. Hermawan, D. Dubé, D. Mantovani, Development of degradable fe-35Mn alloy for biomedical application, *Adv. Mater. Res.* 15–17 (2006) 107–112, <https://doi.org/10.4028/www.scientific.net/amr.15-17.107>.
- [60] International Organization for Standardization, Biological evaluation of medical devices - part 5: tests for in vitro cytotoxicity (ISO 10993-5:2009). [https://books.google.com/books/about/Biological\\_Evaluation\\_of\\_Medical\\_Devices.html?hl=&id=TnA9MwEACAAJ](https://books.google.com/books/about/Biological_Evaluation_of_Medical_Devices.html?hl=&id=TnA9MwEACAAJ), 2009.
- [61] European Powder Metallurgy Association, Euro PM2013 Congress & Exhibition: Compaction, Full Density and Alternative Consolidation, Heat Treatment, European Powder Metallurgy Association, 2013.
- [62] N.M. Daud, N.B. Sing, A.H. Yusop, F.A.A. Majid, H. Hermawan, Degradation and in vitro cell–material interaction studies on hydroxyapatite-coated biodegradable porous iron for hard tissue scaffolds, *J. Orthop. Trauma Transl.* 2 (2014) 177–184, <https://doi.org/10.1016/j.jot.2014.07.001>.
- [63] J. Cheng, T. Huang, Y.F. Zheng, Microstructure, mechanical property, biodegradation behavior, and biocompatibility of biodegradable fe-Fe2O3 composites, *J. Biomed. Mater. Res.* A 102 (2014) 2277–2287.
- [64] E. Zhang, H. Chen, F. Shen, Biocorrosion properties and blood and cell compatibility of pure iron as a biodegradable biomaterial, *J. Mater. Sci. Mater. Med.* 21 (2010) 2151–2163.
- [65] R. Oriňaková, A. Oriňak, M. Giretová, L. Ůbomř Medvecký, M. Kupková, M. Hrubováčková, I. Maskal'ová, J. Macko, F. Kaľavský, A study of

- cytocompatibility and degradation of iron-based biodegradable materials, *J. Biomater. Appl.* 30 (2016) 1060–1070.
- [66] F.L. Nie, Y.F. Zheng, S.C. Wei, C. Hu, G. Yang, In vitro corrosion, cytotoxicity and hemocompatibility of bulk nanocrystalline pure iron, *Biomed. Mater.* 5 (2010), 065015.
- [67] J. Kzhyshkowska, A. Gudima, V. Riabov, C. Dollinger, P. Lavalle, N.E. Vrana, Macrophage responses to implants: prospects for personalized medicine, *J. Leukoc. Biol.* 98 (2015) 953–962.
- [68] B.N. Brown, B.D. Ratner, S.B. Goodman, S. Amar, S.F. Badylak, Macrophage polarization: an opportunity for improved outcomes in biomaterials and regenerative medicine, *Biomaterials* 33 (2012) 3792–3802.
- [69] R. Kardorff, J. Fuchs, M. Peuster, B. Rodeck, Infantile hemangioendothelioma of the liver—sonographic diagnosis and follow-up, *Ultraschall Med.* 22 (2001) 258–264.